Engineering Fracture Mechanics 235 (2020) 107151

Contents lists available at ScienceDirect

Engineering Fracture Mechanics

journal homepage: www.elsevier.com/locate/engfracmech

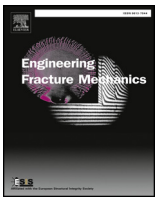

Energy-release rates and opening of cracks in thin barrier coatings on polymer substrates subjected to tensile loading

Marcus Vinícius Tavares da Costa, E. Kristofer Gamstedt*

Uppsala University, Division of Applied Mechanics, Department of Materials Science and Engineering, Box 534, SE-751 21 Uppsala, Sweden

A B S T R A C T

Thin barrier coatings on polymer films are used increasingly in various applications. In coatings development, it is of interest to characterise the fracture toughness. The tensile fragmentation test potentially provides data to determine the critical energy-release rate for channelling cracks in the coatings during crack accumulation with increasing strain. Also, the crack-opening of displacement is of importance to predict barrier properties. In this work, a method based on finite-element simulations is presented to predict the energy-release rate and crack-opening displacement. The results are compared with experimental findings for TiO_2 and mixed TiO_2-Al_2O_3 coatings, with a thickness down to 4–20 nm, on polymer films. It was found that the non-linear stress–strain behaviour of the polymer substrate material needs to be accounted for in the numerical model, in particular for the high strains close to crack saturation observed in these types of materials. Considering the small scales for the cracks and coating thickness, the predicted crack openings compare favourably with those measured experimentally using high-resolution scanning-electron microscopy.

1. Introduction

Thin coatings on polymer substrates have potential use in diverse applications, such food packaging and flexible electronics products. In the food packaging, oxide brittle coatings have interesting properties as barriers [1] that serve to protect food. An example in electronics is optical oxide coatings which provide transparency and electrical conductivity for electronic displays and solar cells [2]. Due to mechanical loads, however, undesirable cracks may form and reduce the functionality of the coatings in both applications [3,4]. In particular for barrier application, the conditions for growth of accumulating cracks and the permeability (controlled by the crack opening) are of special interest.

The accumulation cracking is often empirically characterised by a statistical distribution of coating strength [5–8]. A more physical way to interpret this process would be through fracture mechanics, since cracks are known to initiate and grow from a distribution of defects in the coating. Relatively speaking, the fracture toughness serves as a material parameter rather than strength, which is known to vary with sample dimensions and depend on the geometry, dimensions and orientation of defects.

Crack formation in thin brittle coatings on polymer substrates may be described by fracture mechanics. Fracture mechanics in coating/substrate systems has been studied extensively since the 1990s, where models were developed to determine the energy release rate (ERR) for different kinds of fracture, mainly under elastic conditions and for thicker coatings [9–12]. The present study concerns cracking in ultrathin coatings, with a thickness of 20 nm or less, on inelastic polymer substrates, and focus on channelling cracks. Such cracks propagate in mode I, and accumulate with increasing tensile load where the coating stress is transferred from the stretched substrate through the interface. An example of channelling cracks is shown in the scanning-electron microscopy image of a titanium oxide coating in Fig. 1(a), where the polymer substrate is being stretched while two channelling cracks are propagating between existing cracks. This process is also illustrated schematically in Fig. 1(b). For brittle coatings, the propagation is controlled by the energy released per crack area, quantified by the critical ERR, denoted G_c for the channelling crack in the figure.

* Corresponding author.
E-mail address: kristofer.gamstedt@angstrom.uu.se (E.K. Gamstedt).

https://doi.org/10.1016/j.engfracmech.2020.107151
Received 13 March 2020; Received in revised form 30 April 2020; Accepted 6 June 2020
Available online 10 June 2020
0013-7944/ © 2020 The Authors. Published by Elsevier Ltd. This is an open access article under the CC BY license (http://creativecommons.org/licenses/BY/4.0/).

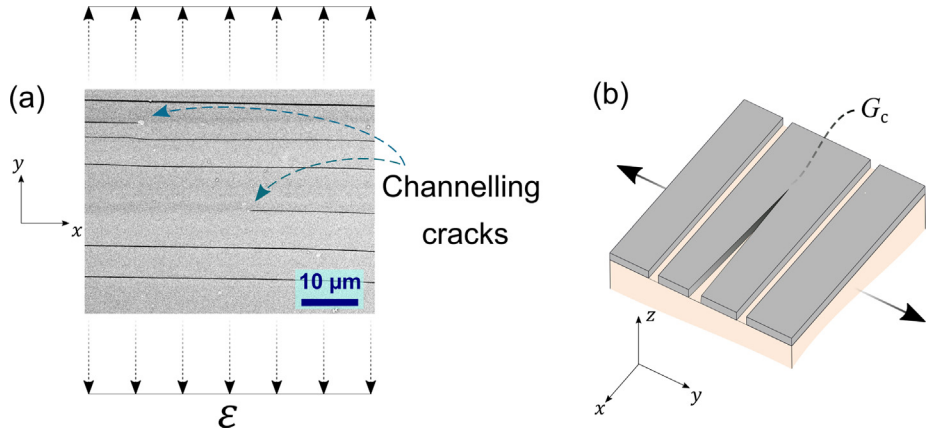

Fig. 1. (a) Two channelling cracks between existing cracks in a titanium oxide coating when applying tensile strain. (b) Schematic illustration of a channelling crack, whose propagation is controlled by the critical ERR, G_c.

This type of fracture traverses through the coating almost instantaneously. When the crack tip is not close to the edges of the sample, the energy release rates becomes independent of the crack length and this condition is known as steady-state cracking [10,13]. Thouless [11] accounted for the interaction of several channelling cracks with different spacing caused by an increasing tensile load. Beuth [12] solved the problem for a single channelling crack accounting for elastic mismatch between coating and substrate [14], with the substrate yield stress incorporated later [15]. Xia and Hutchinson [16] proposed an extension of the elastic mismatch solution for simultaneous and sequential channelling cracks.

These developments are of great value to describe cracking in brittle coatings on elastic or elastic-ideal plastic substrates, and have been applied for coatings with thickness typically above 100 nm and fracture process in small strains [17]. Recent developments in thin film deposition techniques [18] have made it possible to make coatings with a thickness down to a few nanometres on large areas of flexible polymer substrates, which has sparked new applications [19]. When the coatings become more flexible [20], the channelling cracks are observed at higher strains [21], where the stress–strain behaviour of the substrate is appreciably non-linear. The use of a fracture mechanics approach to describe cracking in sub-micron coatings on ductile films necessitates high-magnification electron microscopy, experimental micromechanics (e.g. [8,22,23]) and a generalisation of the modelling framework to account for the non-linear constitutive behaviour of the polymer film. Furthermore, the crack-opening displacement is a key value in predicting barrier properties [3], which is of importance in food packaging applications This value is typically not given directly in the fracture mechanics models, but require a numerical solution even in under simplified elastic conditions [24].

The purpose of this study, is to show a viable path to numerically determine the ERR during the accumulation cracks with increasing tensile strain. The ERR is otherwise normally given at crack onset only [8,17,25]. It is also shown how the average of total crack-opening displacement (COD) can be predicted, which was validated by experimental observations. The COD together with the fragment density are main input parameters for modelling the oxygen-transmission rate (OTR) in the presence of channelling cracks [3]. For food barrier applications, OTR is a commonly used performance indicator, as the oxygen degrades the nutrients. In this sense, the presented work is a step towards predicting the permeability properties relevant in e.g. food packaging applications.

2. Methods

2.1. Materials and fragmentation testing

The experimental investigation using the tensile fragmentation test has been reported in more detail in previous studies [5,26]. The samples were manufactured by roll-to-roll atomic-layer deposition in two types of coating materials [19]. Coatings made of titanium oxide (TiO_2) and mixed oxide (here denoted MOX, composed of TiO_2 and Al_2O_3 of approximately equal amounts) were deposited on the surface of a biaxially oriented poly(ethylene terephthalate) films from Dupont Teijin Melinex ST504 in four configurations: 6 nm and 20 nm for TiO_2, and 4 nm and 20 nm for MOX. The PET film has been stretched during manufacturing and is therefore not in-plane isotropic. Small rectangular specimens from the coated PET films were then examined in-situ during tensile loading in a scanning-electron microscope (SEM), Hitachi TM-1000, equipped with Deben micro-tensile stage to monitor the evolution of channelling cracks in the coating as function of far-field applied tensile strain ε in increments of 1% in strain [8]. The accumulation of cracks was quantified by image analysis at each loading step.

2.2. ERR of channelling cracks

The ERR of steady-state channelling cracks on coatings can be expressed as [27]

$$G_c = \frac{1}{2h_c}\int_0^{h_c} \sigma_c(z)\delta_c(z)dz \tag{1}$$

under plane strain conditions behind the crack front. Here, the strain energy is determined by the work done by the normal stress $\sigma_c(z)$ in the coating needed to produce a crack-opening displacement $\delta(z)$ through the coating thicknessh_c. In our case, the cracks stop at the coating-substrate interface, but there are other cases where cracks can penetrate into the substrate [28,29]. Even though such mechanisms may occur, the ERR can still be determined from virtual crack opening similar to Eq. (1), as exemplified in the case of inelastic deformation in the substrate [15] and for multilayers [30]. It should be noted that Eq. (1) is derived under idealised conditions, such as path independence, elastic behaviour and a well-defined geometry. The effects of these simplifications on the accuracy of ERR predictions is useful topic for future investigations. In the interest of a direct model and employable model, we assume the applicability of Eq. (1) for the coated materials in this investigation.

For cracking in brittle coatings on polymer substrates, it would be useful to predict the ERR accounting for the elastic mismatch and the sequential nature of cracking. The analytical solution by Xia and Hutchinson [16] provides such predictions formulated as

$$G_c = l_0\bar{E}\varepsilon^2\left[2\tanh\left(\frac{l}{2l_0}\right) - \tanh\left(\frac{l}{l_0}\right)\right] \tag{2}$$

where

$$l_0 = \frac{\pi}{2}h_c g(\alpha_D, \beta_D). \tag{3}$$

Here, $\bar{E}$ is the plane strain modulus of the coating, l is the fragment length and the function $g(\alpha_D, \beta_D)$ is a dimensionless function introduced by Beuth [12], dependent only on Dundurs parameters α_D and β_D accounting for the elastic mismatch [14]. Note that Eq. (2) does not account for orthotropic nor non-linear stress–strain behaviour of the substrate, which is frequently the case for coated polymer films. Residual stresses of the coatings were not considered in this work. Here, the temperature of ALD deposition process was 75 °C. As stated in Ref. [8], the crack density of our material system does not substantially change when the ambient temperature varies between 23 °C and 75 °C. In addition, the fragmentation tests were performed months after the coating deposition allowing stress relaxation in the polymer substrate.

2.3. Finite element formulation to determine the ERR

The FE calculations were performed in the solid mechanics module of COMSOL Multiphysics 5.4 using 2D plane-strain conditions. The geometry of this model is shown in Fig. 2. Because of symmetry, it is sufficient only to model half of a fragment length $l/2$ [31,32], where the lighter areas illustrate the other mirrored half of the fragment length. The fragment lengths were experimentally quantified throughout the coating fragmentation test as described above, where the average value is determined as the inverse of the measured crack density $l = 1/\mathrm{CD}(\varepsilon)$, where CD is the crack density given by the number of cracks per unit length.

The superposition principle is used to calculate the ERR in Eq. (1), where $\sigma_c(z)$ is assumed to be the same for the cracked and uncracked coating configurations under steady-state crack conditions [10]. Fig. 2 (a) shows the 2D geometry and the material model of a channelling crack far behind of the crack tip. The two configurations in Fig. 2(b) represents the superposition principle to form the loaded cracked unit cell with no fracture surface tractions in Fig. 2 a). The uncracked illustration to the left in Fig. 2(b) shows how $\sigma_c(z)$ is obtained by prescribing a tensile strain along one boundary of the substrate while symmetry conditions with no displacement [15,33] are set along the opposite boundary (blue line). The fully bonded system is imposed by continuity conditions at the interface since high-resolution SEM have not revealed any measurable debonding close to the coating cracks [22,23]. For the cracked case to the right in Fig. 2(b), the calculated $\sigma_c(z)$ is the crack surface traction in the coating, which is used to calculate the crack-opening displacement $\delta_c(z)$. For both simulations, refined four-node quadrilateral elements were used for the coating and the substrate near interface as Huang et al. [33], rather than default choice eight-node serendipity element [34]. Four-node elements are known to perform better near crack-tip singularities and for non-linear materials found in multilayer structures [35]. In this section, we use FE modelling to estimate the stress in the coating. As an option, there are experimental techniques to measure directly the coating stress state during the fragmentation process e.g. Raman spectroscopy [36] and a synchrotron-based set up [37].

The brittle coatings were considered as linear elastic isotropic materials, where their Young's moduli E_c were measured by atomic force microscopy [22], and Poisson ratiosν_c were estimated in Ref. [22]. Although polymer substrates exhibit non-linear behaviour dependent on strain rate, temperature, stress history, finite deformation etc., e.g. [38], we chose to an elastic-nonlinear plastic model corresponding to the stress–strain behaviour determined experimentally at approximately the same rate and temperature as the fragmentation test. Orthotropic elasticity is combined with a nonlinear user-defined plastic-strain hardening function, which has been shown to follow the experimental stress–strain measurements accurately for the polymer film, even if based on small deformation theory [23]. All tests were done under constant strain rates and constant ambient temperature [8,22,23]. The orthotropic material model of the polymer substrate was calibrated from tensile tests along the two main material axes using a Shimadzu Autograph AGS-X tensile machine with in-situ measurements of the 2D strain field with digital-image correlation (DIC) using the GOM Aramis stereo system 5 M, and subsequently implemented in COMSOL [23]. Despite using the elastic–plastic material model for the substrate, the energy dissipated in substrate plasticity in the superposition approach is neglected for simplicity. A possible way to incorporate this effect can be found in Ref. [31].

Typically, the coating thickness is negligible compared with that of the substrate for these ultrathin coating systems. As pointed

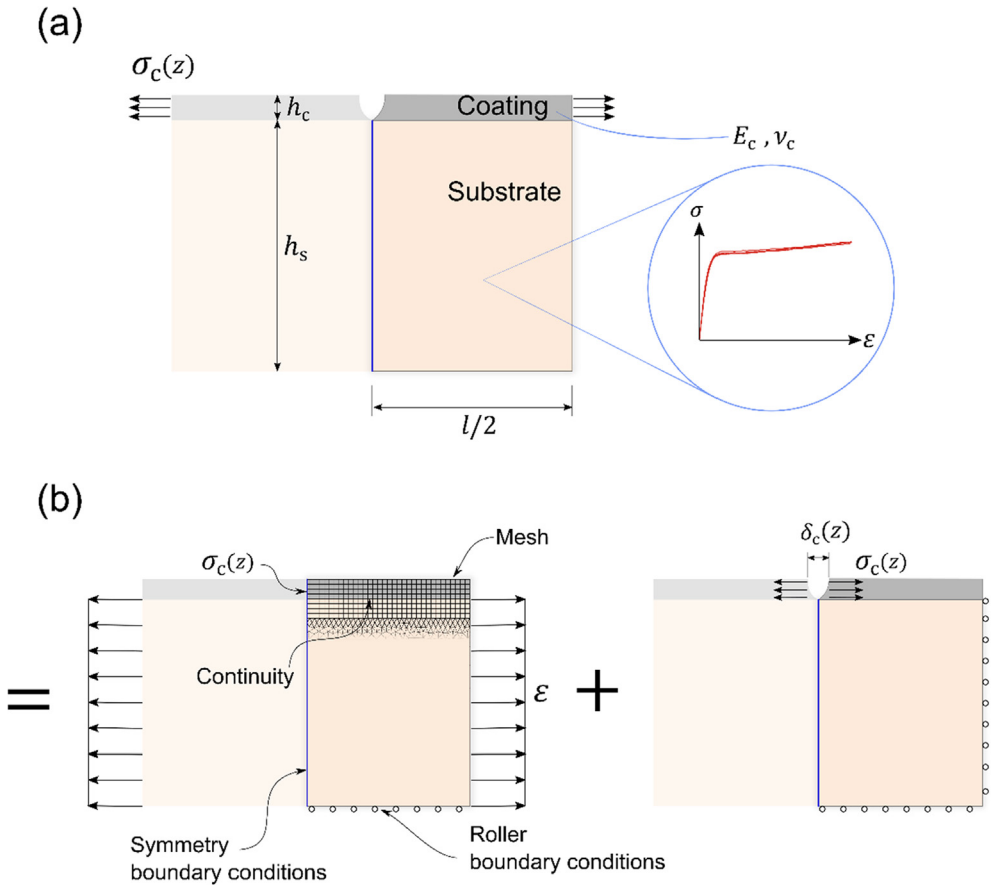

Fig. 2. (a) Geometry of a channelling crack far behind the crack tip and the material model used for the coating and substrate. (b) The boundary conditions used in the superposition FE model. The horizontal boundaries of the unit cell remain straight, with a uniform far-field deformation of the coating and substrate.

out by Begley and Hutchinson [27], the ERR is sensitive to the relative thickness of the substrate to that of the coating, e.g. h_s/h_c, in particular for the case of large elastic mismatches. For computational reasons to reduce the number of degrees of freedom, one would like limit the amount of substrate material in the model while still obtaining accurate estimates of the ERR without any edge effects. Therefore, a sensitivity analysis of thickness ratio h_s/h_c was performed in the FE model to avoid any edge effects from the reduced thickness before computing the final values for the ERR.

2.4. Finite element formulation to determine the crack-opening displacement

The crack-opening displacement (COD) after the fragmentation process is of high engineering importance since it controls the barrier properties, such as the oxygen transmission rate. The deformation of the substrate has a strong effect on the crack opening.

The crack opening shown in Fig. 2 is used to calculate the ERR at steady-state crack growth. The COD is substantially larger after the fragmentation process than during crack growth. The increased COD is attributed to the deformation of the substrate, especially near the crack. To allow for this substrate deformation, contact elements are introduced at the coating-substrate interface. These elements are equipped with linear cohesive springs, which can incorporate local deformations at the interface not captured for shared nodes and displacement continuity used in instantaneous cracking in Fig. 2. Since no opening debonding at the coating-substrate interface was detected in the SEM analyses, only the shearing mode contact penalty stiffness, K_τ, was used as a tuning parameter with the substrate and coating remaining in contact. The value of K_τ was chosen to be the smallest value for which the ERR is constant and independent of K_τ. Using these contact elements, the COD was finally predicted using the geometry and boundary conditions shown schematically in Fig. 3.

2.5. Experimental setup for the crack-opening displacement measurements

This section presents a way to estimate the COD from a crack formed at crack onset strain. The samples were stretched up to saturation stage and then examined in SEM. The largest cracks found were measured as described below. Those are the early cracks

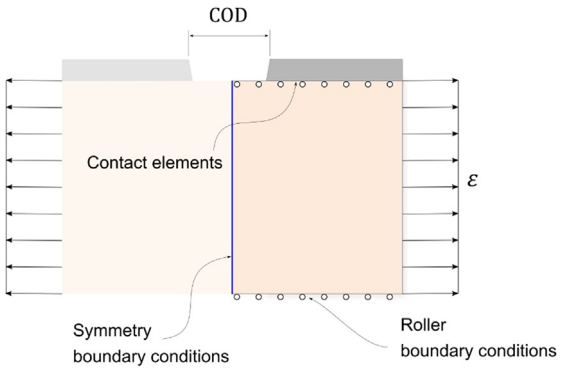

Fig. 3. Geometry and boundary conditions used in the FE model for COD.

formed at crack onset strain.

The samples were prepared as described in Refs. [8,22], and stretched using a Deben tensile stage with a deformation rate of 1.0 mm/min up to crack saturation. Before the tests, the sample were also coated with an Au-Pd conductive coating using a Quorum Polaron SC7640 sputter coater to minimize charging effects and make the cracking process clearly visible during fragmentation. The conductive layer only had limited influence on the cracking process in the metal-oxide coatings [22]. Right after the stretching, the samples were brought straight away to a high-resolution scanning electron microscopy (SEM) a Zeiss 1530 field emission gun equipped with an in-lens secondary electron detector and operating at 5 kV of acceleration voltage to examine in detail the opening of the channelling cracks. In our case, the highly strained samples did not shrink measurably when taken from the tensile stage, indicating that most of strain was plastic, and the measured COD can be compared to the numerical predictions. The close-up SEM images were taken randomly from different cracks located throughout the sample surface. The images were binarised in Matlab to measure the crack opening. The threshold value was adjusted by comparing the greyscale images with the binarised black-and-white images and making sure that all cracks were well-defined with their proper openings. A script was made to count the number of black pixels NP, corresponding to the crack opening, and the number of cracks NC, along five lines extending over the entire image and perpendicular to the cracks. The average COD can simply be estimated as

$$\mathrm{COD} = \eta \frac{\mathrm{NP}}{\mathrm{NC}} \tag{4}$$

where η is the width of one pixel, determined from a well-defined reference length. The SEM images did not indicate any V-shaped crack profile, and were therefore assumed to have a relatively rectangular profile, as schematically illustrated in Fig. 3.

3. Results and discussion

3.1. Effect of thickness ratio on the ERR of channelling cracks

The first step is to assure ERR convergence and reduce the computational cost by decreasing the relative substrate thickness. Fig. 4 shows how the thickness of the substrate affects the ERR of the coating at crack onset. For all coating configurations, the solutions differ by 7% from 5 to 250 of substrate-to-coating thickness ratio, h_s/h_c. The variation becomes less than 1% when thickness ratio is

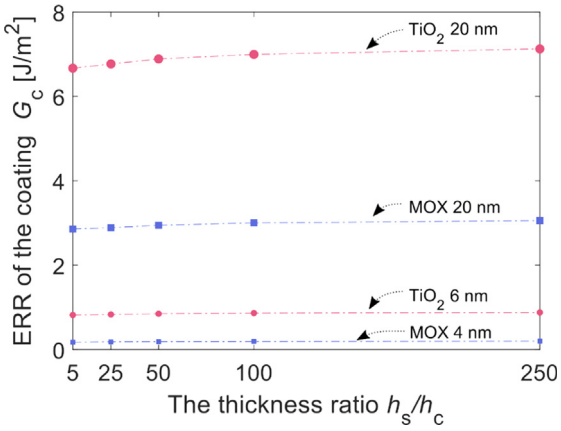

Fig. 4. Effect of relative substrate thickness on the ERR determined from the FE model.

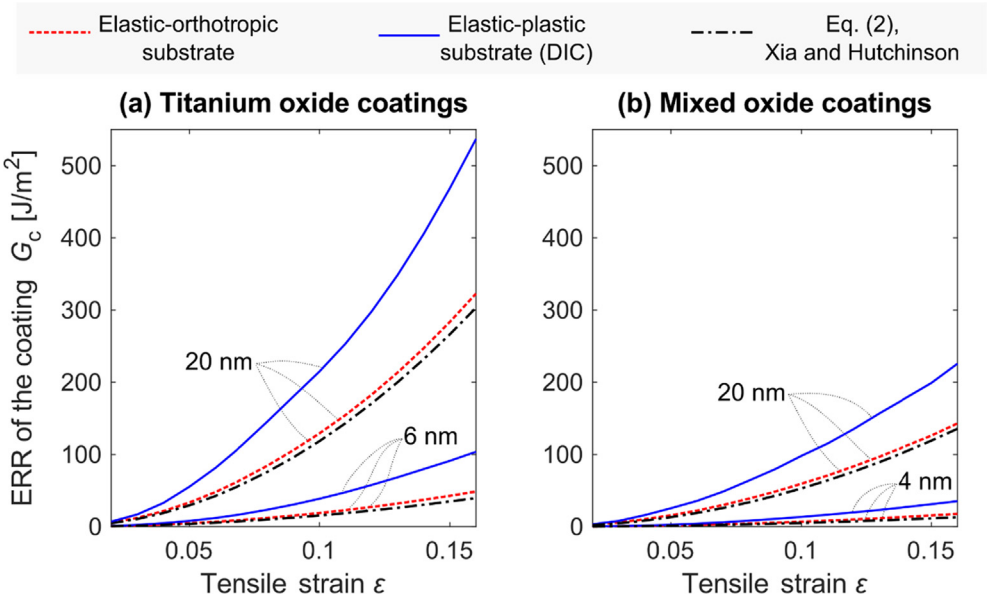

Fig. 5. Calculated ERR for (a) TiO_2 and (b) MOX coatings with respect to tensile strain.

larger than 50. A thickness ratio of 50 was therefore chosen for all remaining simulations in this study. In comparison, Huang et al. [33] found 20 as a sufficient h_s/h_c ratio for their numerical work. Toth et al. [39] performed their calculations for a chromium coating of 100 nm thick with 28 as their thickness ratio. In our system, the higher elastic mismatch led to a thickness ratio that is about twice as high. Higher ratios up to the limit with the real thickness of the substrate do not affect the ERR [30,40], but require significantly longer calculation times and mesh refinements.

3.2. ERR calculation as a function of the applied tensile strain

Fig. 5. shows the final calculations for ERR of the coatings with respect to applied tensile strain, where the FE results for elastic and inelastic substrates are compared to the analytical solution in Eq. (2). The numerical elastic solutions in red are slightly higher than the analytical solutions, most likely due to the orthotropic substrate used in the FE simulations. For isotropic substrates, those solutions are effectively the same. The degree of orthotropy is relatively low for the investigated bioaxially oriented PET film [23]. For higher degrees of orthotropy, e.g. in extruded polymer films stretched onto a roll winder, a model based on the assumption of an isotropic substrate will be less precise. The notable difference in ERR is when the non-linear inelastic behaviour of the substrate is accounted for (cf. blue line). In this case, the ERR is considerably higher than elastic solutions for large strains. This higher trend was also found by Beuth and Klingbeil [15] due to substrate plasticity. The ERR values were higher for the TiO_2 coatings than that of MOX coatings, mainly because the higher Young's modulus of the TiO_2 coatings [22]. The stiffer coating systems also exhibit a larger difference compared with the elastic solution, which can be attributed to the higher elastic mismatch. It can be noted that the shape of the numerical plots in Fig. 5 is essentially quadratic, just like analytical expression in Eq. (2). Finally, it should be pointed out that it is possible to numerically estimate the ERR for channelling cracks in coated films exhibiting a non-linear stress–strain relationship, which is significantly different from analytical predictions based on linear elastic fracture mechanics. This means that it is possible to investigate how the critical ERR, G_c, evolves during crack accumulation as the applied strain is increased. In some previous works, e.g. [8,17,25], G_c has been determined from crack onset only, i.e. at the appearance of the very first crack, which is controlled by the most severe defect, and hence subject to considerable scatter.

3.3. Contact penalty stiffness

In the ERR simulations, steady-state crack growth is assumed, with perfect adhesion between the coating and substrate. After crack formation and further straining, the cracks were observed with in-situ SEM to open, which means that partial slipping at the interface must occur. In order to estimate the crack opening, this mechanism is here accommodated by a contact penalty stiffness at the interface ranging from 1.0×10^{14} to 4.0×10^{16} N/mm^3. The sensitivity of this parameter on the targeted COD is of interest. However, we chose to investigate the sensitivity with regard to the coating stress at crack onset, since the sensitivity with respect to the COD showed the same behaviour and it is numerically more convenient to calculate the coating stress. The coating stress and COD are the key parameters for technical applications, since the coating stress affects further cracking and the COD affects the barrier performance.

The influence of the contact stiffness on the coating stress at crack onset is shown in Fig. 6. The coating stress with a penalty stiffness below 10^{14} N/mm^3 shows a very high dependence on the penalty stiffness, and is not plotted in the figure. For higher values

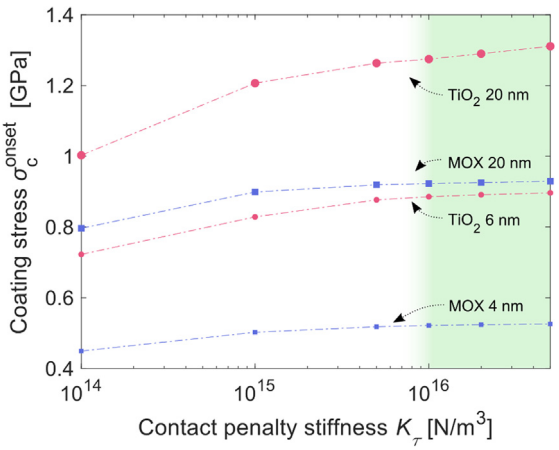

Fig. 6. Effect of contact penalty stiffness on the coating stress at crack onset determined from the FE model for COD calculations.

of the contact stiffness representing a more bonded interface, the computational times increases significantly. Beyond 4.0 × 10^{16} N/mm^3, our FE calculations did not even converge. For contact penalty stiffness in the range between 1.0 × 10^{16} and 4.0 × 10^{16} N/mm^3, the stress in the coating becomes relatively invariant within a range of about 2%. This reasonably uniform region is highlighted in green in Fig. 6. The same near-invariance was also observed for the COD in this range. We therefore chose a contact stiffness of 4.0 × 10^{16} N/mm^3 for further calculations, since it belongs to the stable range and represents a well-bonded interface. Incidentally, the maximum shear stress using the green range for contact stiffness is close to interfacial shear strength determined from saturation in a fragmentation test using a shear-lag model [8].

3.4. Crack opening

Finally, the calculated values of the COD with respect to applied strain is presented in Fig. 7. The calculations were made with a contact stiffness of 4.0 × 10^{16} N/mm^3, belonging to the range where converging results and relatively invariant CODs and coating stresses (the green field in Fig. 6). As can be seen in Fig. 7, the CODs increase with increasing strain all the way up to crack-saturation strains. The unevenness in the curves stems from the scatter in the experimental data of crack density vs. strain. The TiO_2 coatings generally have larger CODs than MOX coatings, due to the higher coating-substrate stiffness mismatch in the TiO_2 systems. In addition, there is a colour plot inserted in Fig. 7. It shows a close-up of the shear stress field near the cracked thicker TiO_2 coating at the maximum strain. The cracks shows straight edges with a negligible inclination angle, meaning that the COD here determined on the top of the coating is representative for the entire coating. A uniform COD profile, i.e. not V-shaped, means that one representative COD value can be used in the estimations of transport properties, such as moisture diffusion, oxygen transmission rates, etc. [3,41].

3.5. Comparison with experimental crack-opening measurements

A set of SEM images for all cracked coating materials are shown in Fig. 8. Here, we focus on the thickness of the near horizontal lines, representing cracks in the coatings perpendicular to the loading direction. The light vertical features in the TiO_2 coatings correspond to ridged cracks, which have been analysed in another study [23]. In the magnified images, tortuous cracks patterns can

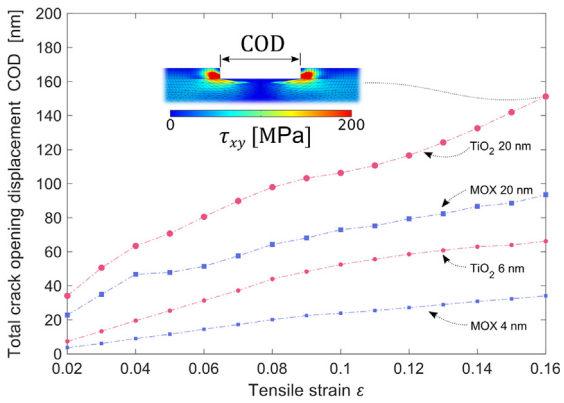

Fig. 7. Calculated COD for (a) TiO_2 and (b) MOX coatings with respect to tensile strain.

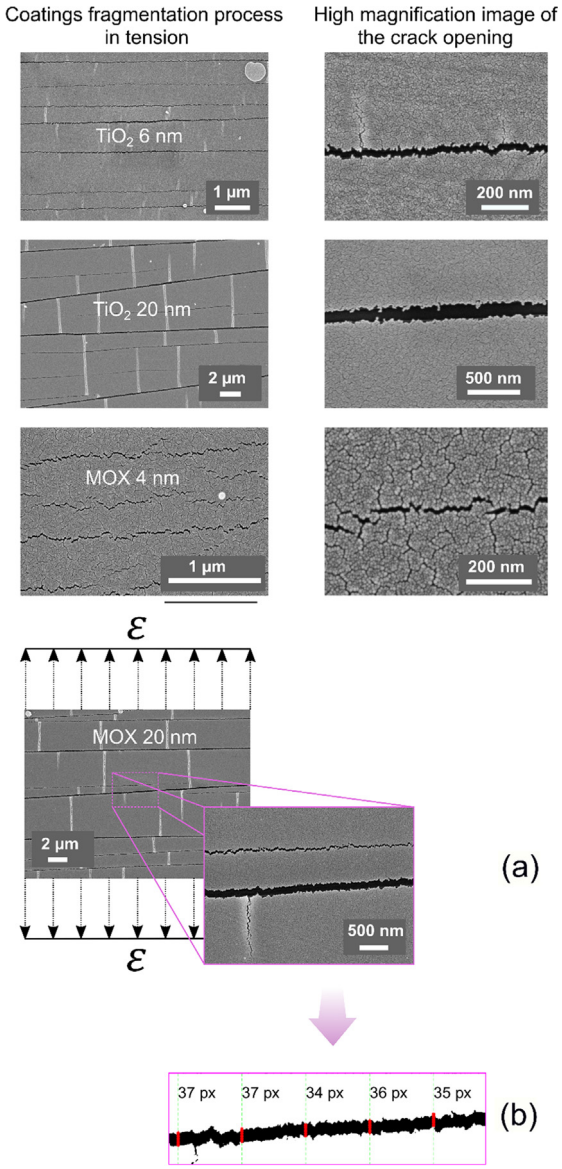

Fig. 8. Set of SEM images from the samples stretched up to 16% of tensile strain, where crack saturation has been reached. (a) Close-up of a cracked 20 nm MOX coating and (b) from which a binarised image is used to determine the COD in terms of pixels.

be observed, especially for the thinner MOX coating. On this lengthscale and for such thin coatings, the material cannot be considered as homogenous but is appreciably heterogeneous. The SEM images also show that the crack opening is can vary considerably from crack to crack. Cracks that are formed early at relatively low strains eventually show larger CODs than those formed more recently at higher strains. This variation was stronger for the thicker coatings than for the thinner ones.

The image post-processing to measure the COD is also shown Fig. 8; from (a) where the image of the stretched thicker MOX coating is magnified along a crack, to (b) where pixels spanning the crack are counted in the binarised image. The COD is then converted to length unit through Eq. (4). The COD average for each crack was determined for at least 36 measurements in the interest of statistical significance. The constitutive stress–strain behaviour of the polymer substrate used in the FE model was characterised under quasi-static conditions [23]. For the thicker coatings, only the wider cracks formed at onset were analysed, since polymer film close to these cracks show a more similar loading history and strain rate as in the quasi-static characterisation step, compared with the dynamic situation of recently formed cracks a high strains with limited relaxation time.

Fig. 9 presents comparisons between experimentally measured and numerically predicted CODs. The error bars represent the standard deviation. There is a reasonable agreement for the thicker coatings. For the thinner coatings, the difference is larger, although the values are within the same order of magnitude. A reason for the larger difference could be the limitations in resolution and effects of charging at high magnification. Also, the thinner coatings show wavier crack, which is not accounted for in the

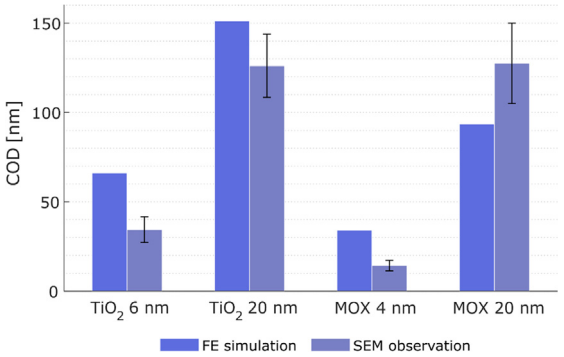

Fig. 9. Comparison of the CODs from numerical predictions and from experimental measurements in SEM.

idealised FE model. Nevertheless, we claim that the presented method shows a predictive potential, which could eventually be used estimate the COD and ultimately also resultant barrier properties.

4. Concluding remarks

In this work, the fracture process in titanium oxide and mixed titanium/aluminium oxide coatings on polymer substrates has been investigated, both experimentally and numerically. The investigated coatings were very thin, down to 4–20 nm, and the strains at crack saturation were relatively high, up to 0.16. These conditions mean special requirements on predictive approaches, and well-established analytical relations may not be suitable, and a numerical approach is necessary.

A scheme has been shown how to determine the ERR as a function of applied tensile strain, based on the superposition principle. Thus, not only the typical critical ERR at crack onset can be characterised from fragmentation test, but also how this property changes with increasing strain in successively shorter fragments. Tensile testing have shown that the polymer substrates exhibit a significantly non-linear stress–strain relationship. Analytical predictions of the ERR based on linear elasticity differed considerably from that based on FE simulations using the non-linear substrate material model. Therefore, it is recommended to resort to a numerical approach in cases with large strains where the constitutive behaviour of the polymer substrate is markedly non-linear. For ultrathin coatings, the coating to substrate thickness ratio is small, and the substrate thickness was reduced to save computational time.

The ERR calculations dealt with the propagation of a channelling crack under steady-state conditions. In this instantaneous crack growth, the interface was considered to be perfectly bonded. As the samples were stretched, the cracks were seen to open measurably with straight crack edges. Effectively, this means that coating and substrate are not perfectly bonded at the crack tip at this stage of the tensile test. In order to calculate the COD, the necessary local interfacial slippage was accommodated by shear springs at the interface, defined by a local penalty stiffness. The stiffness parameter was tuned to get converging results in terms of coatings stress.

The crack density and COD are the key parameters that impair barrier performance. The CODs were predicted numerically, and were shown to give a reasonable correlation with experimentally quantified CODs using high-resolution SEM, in particular for the thicker coatings (20 nm). This suggests some promise of a viable procedure to predict COD, and ultimately also barrier properties, even for very thin coatings on polymer films.

Declaration of Competing Interest

The authors declare that they have no known competing financial interests or personal relationships that could have appeared to influence the work reported in this paper.

Acknowledgements

Financial support and supply of the test samples for this study by Tetra Pak Packaging Solutions AB are acknowledged. MVTdC is grateful to the European Commission within the framework of the Erasmus Mundus Programme, Action 2-STRAND 1, Lot 9, Brazil for partial financial support of his PhD studies. The authors would like to thank Dr. Jessica Bolinsson and Dr. Eskil Andreasson for the valuable scientific discussions. We would also like to acknowledge Professor emeritus Bengt Lundberg for revising the manuscript.

References

[1] Henry BM, Erlat AG, McGuigan A, Grovenor CRM, Briggs GAD, Tsukahara Y, et al. Characterization of transparent aluminium oxide and indium tin oxide layers on polymer substrates. Thin Solid Films 2001;382:194–201. https://doi.org/10.1016/S0040-6090(00)01769-7.
[2] Cheng I-C, Wagner S. Overview of flexible electronics technology. Boston: Springer; 2009.
[3] Yanaka M, Henry BM, Roberts AP, Grovenor CRM, Briggs GAD, Sutton AP, et al. How cracks in SiO_x-coated polyester films affect gas permeation. Thin Solid Films 2001;397:176–85. https://doi.org/10.1016/S0040-6090(01)01473-0.
[4] Mora A, Khan KA, El Sayed T. Prediction of crack density and electrical resistance changes in indium tin oxide/polymer thin films under tensile loading. Int J

Damage Mech 2015;24:546–61. https://doi.org/10.1177/1056789514539362.
[5] Leterrier Y, Wyser Y, Månson JAE, Hilborn J. A method to measure the adhesion of thin glass coatings on polymer films. J Adhes 1994;44:213–27. https://doi.org/10.1080/00218469408027078.
[6] Leterrier Y, Boogh L, Andersons J, Månson J-AE. Adhesion of silicon oxide layers on poly(ethylene terephthalate). I: Effect of substrate properties on coating's fragmentation process. J Polym Sci, Part B: Polym Phys 1997;35:1449–61. https://doi.org/10.1002/(SICI)1099-0488(19970715)35:9%3C1449:: AID-POLB15%3E3.0.CO;2-6.
[7] Leterrier Y, Andersons J, Pitton Y, Månson J-AE. Adhesion of silicon oxide layers on poly(ethylene terephthalate). II: Effect of coating thickness on adhesive and cohesive strengths. J Polym Sci, Part B: Polym Phys 1997;35:1463–72. https://doi.org/10.1002/(SICI)1099-0488(19970715)35:9<1463:: AID-POLB16>3.0.CO;2-4.
[8] Tavares da Costa MV, Bolinsson J, Neagu RC, Fayet P, Gamstedt EK. Experimental assessment of micromechanical models for fragmentation analysis of thin metal oxide coatings on polymer films under uniaxial tensile deformation. Surf Coat Technol 2019;370:374–83. https://doi.org/10.1016/j.surfcoat.2019.03.035.
[9] Hutchinson JW, Suo Z. Mixed mode cracking in layered materials. Adv Appl Mech 1991:63–191. https://doi.org/10.1016/S0065-2156(08)70164-9.
[10] Evans AG, Drory MD, Hu MS. The cracking and decohesion of thin films. J Mater Res 1988;3:1043–9. https://doi.org/10.1557/JMR.1988.1043.
[11] Thouless MD. Crack spacing in brittle films on elastic substrates. J Am Ceram Soc 1990;73:2144–6. https://doi.org/10.1111/j.1151-2916.1990.tb05290.x.
[12] Beuth JL. Cracking of thin bonded films in residual tension. Int J Solids Struct 1992;29:1657–75. https://doi.org/10.1016/0020-7683(92)90015-L.
[13] Nakamura T, Kamath SM. Three-dimensional effects in thin film fracture mechanics. Mech Mater 1992;13:67–77. https://doi.org/10.1016/0167-6636(92)90037-E.
[14] Dundurs J. Discussion Edge-bonded dissimilar orthogonal elastic wedges under normal and shear loading (Bogy, D. B., 1968, ASME J. Appl. Mech., 35, pp. 460–466). J Appl Mech 1969;36:650–2. https://doi.org/10.1115/1.3564739.
[15] Beuth JL, Klingbeil NW. Cracking of thin films bonded to elastic-plastic substrates. J Mech Phys Solids 1996;44:1411–28. https://doi.org/10.1016/0022-5096(96)00042-7.
[16] Xia ZC, Hutchinson JW. Crack patterns in thin films. J Mech Phys Solids 2000;48:1107–31. https://doi.org/10.1016/S0022-5096(99)00081-2.
[17] Choi Y-H, Bulliard X, Benayad A, Leterrier Y, Månson J-AE, Lee K-H, et al. Design and fabrication of compositionally graded inorganic oxide thin films: Mechanical, optical and permeation characteristics. Acta Mater 2010;58:6495–503. https://doi.org/10.1016/j.actamat.2010.08.011.
[18] Ohring M. Materials science of thin films. Elsevier Science & Technology; 2001.
[19] Dickey E, Barrow WA. High rate roll to roll atomic layer deposition, and its application to moisture barriers on polymer films. J Vac Sci Technol, A 2012;30:021502. https://doi.org/10.1116/1.3678486.
[20] Bishop A, Roll-to-roll C. vacuum deposition of barrier coatings. Wiley; 2010.
[21] Yanaka M, Miyamoto T, Tsukahara Y, Takeda N. In situ observation and analysis of multiple cracking phenomena in thin glass layers deposited on polymer films. Compos Interfaces 1998;6:409–24. https://doi.org/10.1163/156855499X00116.
[22] Tavares da Costa MV, Neagu C, Fayet P, Wiklund U, Li H, Leifer K, et al. Comparison of test methods estimating the stiffness of ultrathin coatings. J Coat Technol Res 2018;15:743–52. https://doi.org/10.1007/s11998-018-0085-0.
[23] Tavares da Costa MV, Bolinsson J, Fayet P, Gamstedt EK. Transverse ridge cracking in tensile fragmentation tests of thin brittle coatings on polymer substrates. Surf Coat Technol 2020;382:125025. https://doi.org/10.1016/j.surfcoat.2019.125025.
[24] Xie C, Tong W. Cracking and decohesion of a thin Al_2O_3 film on a ductile Al–5%Mg substrate. Acta Mater 2005;53:477–85. https://doi.org/10.1016/j.actamat.2004.10.005.
[25] Andersons J, Modniks J, Leterrier Y, Tornare G, Dumont P, Månson J-AE. Evaluation of toughness by finite fracture mechanics from crack onset strain of brittle coatings on polymers. Theor Appl Fract Mech 2008;49:151–7. https://doi.org/10.1016/j.tafmec.2007.11.002.
[26] Aveston J, Cooper GA, Kelly A. Single and multiple fracture. The properties of fiber composites conference proceedings. 1971. p. 15–26.
[27] Begley MR, Hutchinson JW. The mechanics and reliability of films, multilayers and coatings. Cambridge University Press; 2017.
[28] Thouless MD, Li Z, Douville NJ, Takayama S. Periodic cracking of films supported on compliant substrates. J Mech Phys Solids 2011;59:1927–37. https://doi.org/10.1016/j.jmps.2011.04.009.
[29] Kim K, Luo H, Zhu T, Pierron ON, Graham S. Influence of polymer substrate damage on the time dependent cracking of SiN_x barrier films. Sci Rep 2018;8:1–9. https://doi.org/10.1038/s41598-018-22105-2.
[30] Meng F, David JL, Bollin S, Nichols ME, Thouless MD. Kinetics of channeling cracks in polymeric coatings. Int J Solids Struct 2018;132–133:105–13. https://doi.org/10.1016/j.ijsolstr.2017.09.023.
[31] Jansson NE, Leterrier Y, Månson J-AE. Modeling of multiple cracking and decohesion of a thin film on a polymer substrate. Engng Fract Mech 2006;73:2614–26. https://doi.org/10.1016/j.engfracmech.2006.04.013.
[32] Peng C, Jia Z, Bianculli D, Li T, Lou J. In situ electro-mechanical experiments and mechanics modeling of tensile cracking in indium tin oxide thin films on polyimide substrates. J Appl Phys 2011;109:103530. https://doi.org/10.1063/1.3592341.
[33] Huang ZY, Huang R, Prévost JH, Suo Z. Channel-cracking of thin films with the extended finite element method. Eng Fract Mech 2003;70:2513–26. https://doi.org/10.1016/S0013-7944(03)00083-3.
[34] Ergatoudis I, Irons BM, Zienkiewicz OC. Curved, isoparametric, "quadrilateral" elements for finite element analysis. Int J Solids Struct 1968;4:31–42. https://doi.org/10.1016/0020-7683(68)90031-0.
[35] Begley MR, Begley CJ. Interfacial debonding around rectangular features in multilayer structures. Interface Sci 2003;11:319–27. https://doi.org/10.1023/A:1025148423632.
[36] Ahmed F, Bayerlein K, Rosiwal SM, Göken M, Durst K. Stress evolution and cracking of crystalline diamond thin films on ductile titanium substrate: Analysis by micro-Raman spectroscopy and analytical modelling. Acta Mater 2011;59:5422–33. https://doi.org/10.1016/j.actamat.2011.05.015.
[37] Gruber PA, Arzt E, Spolenak R. Brittle-to-ductile transition in ultrathin Ta/Cu film systems. J Mater Res 2009;24:1906–18. https://doi.org/10.1557/jmr.2009.0252.
[38] Bergström JS, Bischoff JE. An advanced thermomechanical constitutive model for UHMWPE. Int J Struct Changes Solids 2010;2:31–9.
[39] Toth F, Rammerstorfer FG, Cordill MJ, Fischer FD. Detailed modelling of delamination buckling of thin films under global tension. Acta Mater 2013;61:2425–33. https://doi.org/10.1016/j.actamat.2013.01.014.
[40] Rehman Hu, Ahmed F, Schmid C, Schaufler J, Durst K. Study on the deformation mechanics of hard brittle coatings on ductile substrates using in-situ tensile testing and cohesive zone FEM modeling. Surf Coat Technol 2012;207:163–9. https://doi.org/10.1016/j.surfcoat.2012.06.049.
[41] Gagani AI, Echtermeyer AT. Fluid diffusion in cracked composite laminates – Analytical, numerical and experimental study. Compos Sci Technol 2018;160:86–96. https://doi.org/10.1016/j.compscitech.2018.03.025.